Supporting Information

Wong et al. 10.1073/pnas.1018927108

SI Materials and Methods

Parasite Imaging. Samples for immunofluorescence microscopy (IFA) were probed with relevant primary and secondary antibodies before mounting in VectaShield (Vector Laboratories) with 0.1 ng/μL DAPI (Invitrogen). Fluorescence images were obtained using a Plan-Apochromat 100×/1.40 oil immersion phase-contrast lens (Zeiss) on an AxioVert 200M microscope (Zeiss) equipped with an AxioCam Mrm camera (Zeiss). Invasion images were acquired as Z-stacks taken above and below parasites and processed using the Axiovision release 4.8 deconvolution software package. Primary antibodies used were raised against recombinant *Plasmodium falciparum* actin-depolymerizing factor 1 (PfADF1) (1:300); *PfAct1* (1:300) (1), and *P. falciparum* rhoptry neck protein 4 (1:200) (2) followed by probing with appropriate Alexa Fluor 488/594 secondary antibodies (Molecular Probes).

SDS/PAGE and Immunoblotting. *P. falciparum* parasite pellets from saponin-treated schizonts were solubilized in 2× SDS loading buffer and separated on 4–12% (Bis-Tris) SDS-NuPAGE gels (Invitrogen) under reducing conditions. Immunoblotting was performed according to standard protocols. Nitrocellulose membranes were blocked in 10% (wt/vol) skim milk, 0.1% Tween 20-PBS for 1 h and probed with primary antisera [rabbit anti-PfADF1 (1:1,000), rabbit anti-PfAct1 (1:500) (1), rabbit anti-*P. falciparum* aldolase (3) (1:1,000), and rabbit anti- *P. falciparum* apical membrane antigen 1 (1:1,000) (4)] in 1% milk, 0.1% Tween 20-PBS for 1 h. After two washes membranes were incubated with appropriate secondary antibodies (Millipore) for 1 h and developed by ECL (Amersham Biosciences). Hypotonic solubilization of parasite samples followed (5).

Actin-Depolymerizing Factor/Cofilin Protein Cloning, Expression, and Purification. Full-length *PfADF1*, *P. falciparum* actin-depolymerizing factor 2 (*PfADF2*), and *Homo sapiens* cofilin (HsCOF) were amplified from *P. falciparum* and human cDNA, respectively (all primers are available on request). PfADF1.K72A, HsCOF-Pf, and PfADF1-Hs chimeric actin-depolymerizing factor/cofilin (AC) proteins were ordered synthetically (GeneArt). Purified and digested products were ligated into the BamHI/XhoI site of the pGEX4T vector (GE Healthcare) to generate recombinant proteins with an N-terminal GST fusion tag and transformed into DH10β *Escherichia coli* competent cells (Invitrogen). Sequence-positive clones were retransformed into BL-21 (DE3) *E. coli* cells for protein expression. Expression of GST-PfADF1, GST-PfADF2, and PfADF1.K72A was induced by the addition of 1 mM isopropyl β-D-1-thiogalactopyranoside (IPTG) when the culture reached an OD_{600} of 0.6. After the addition of IPTG, cultures were grown for 4 h at 37 °C; then cells were harvested and ruptured by sonication with fusion protein purified using glutathione agarose (Sigma) in lysis buffer [20 mM Tris (pH8), 300 mM NaCl, 0.3% Triton X-100, 5 mM 2-mercaptoethanol, and 0.02% NaN_3) supplemented with complete protease inhibitor (Roche Applied Science). After extensive washes in wash buffer 1 [20 mM Tris (pH8), 1 M NaCl, 2% Triton X-100, 5 mM 2-mercaptoethanol, and 0.02% NaN_3) and 2 [20 mM Tris (pH8), 1 M NaCl, 5 mM 2-mercaptoethanol, and 0.02% NaN_3], protein was eluted [20 mM Tris [pH8], 150 mM NaCl, 0.3% Triton X-100, 20 mM glutathione, and 0.02% NaN_3]. Purified proteins were dialyzed overnight into T-buffer [20 mM Tris (pH8), 100 mM NaCl, 5 mM $CaCl_2$ and 5% glycerol] with the N-terminal GST tag removed by thrombin protease (GE Healthcare) treatment followed by size-exclusion chromatography using a Superdex S200 10/300 GL column (GE Healthcare) with 20 mM Tris (pH8), 10 mM NaCl, 5 mM 2-mercaptoethanol and 0.02% NaN_3 as elution buffer. Protein purity was assessed by SDS/PAGE.

PfAct1 Cloning, Expression, and Purification. Full-length *P. falciparum* actin1 (*PfAct1*) was amplified (all primers are available on request), and digested products were ligated into the Nde1/Xho1 site of the pET28 vector (Novagen) to generate recombinant proteins with an N-terminal hexa-His fusion tag and transformed into DH10β *E. coli* competent cells (Invitrogen). Sequence-positive clones were transformed into Rosetta 2 (DE3) *E. coli* cells for protein expression. Expression of PfAct1 was induced by the addition of 1 mM IPTG when the culture reached an OD_{600} of 0.6. After the addition of IPTG cultures were grown for 4 h at 37 °C; then cells were harvested and ruptured by sonication. Soluble proteins were separated from the inclusion body, which contains the expressed $His_{6\times}$-PfAct1, by centrifugation at 30,000 × *g* at 4 °C for 30 min. The inclusion body was solubilized in solubilization buffer [6 M guanidine hydrochloride, 50 mM Tris (pH 8), 0.3 M NaCl, and 10 mM 2-mercaptoethanol] at 25 °C for 1 h with rocking. Solubilized $His_{6\times}$-PfAct1 was purified in denatured condition by incubating with NiNTA agarose (Qiagen) at 4 °C for 1 h with rocking. Proteins were washed initially with wash buffer 1 [6 M guanidine hydrochloride, 50 mM Tris (pH 8), 0.3 M NaCl, 30 mM imidazole, and 10 mM 2-mercaptoethanol] followed by refolding via washing the protein-bound agarose with refolding buffer [20 mM Tris (pH 8), 0.1 mM $CaCl_2$, 0.1 mM ATP, and 5 mM 2-mercaptoethanol]. $His_{6\times}$-PfAct1 was eluted in elution buffer [20 mM Tris (pH8), 0.1 mM $CaCl_2$, 0.1 mM ATP, 250 mM imidazole, and 5 mM 2-mercaptoethanol]. Purified protein was concentrated and further purified by size-exclusion chromatography using a Superdex S200 10/300 GL column (GE Healthcare) with 20 mM Tris (pH8) 0.1 mM $CaCl_2$, 0.1 mM ATP, and 5 mM 2-mercaptoethanol as elution buffer. Protein purity was assessed by SDS/PAGE.

PfADF1 Structure Determination and Refinement. The structure factors were provided as input into the BALBES server (6). A molecular replacement solution was found by the program Molrep (7) using the coordinates of AtADF (PDB ID code 1F7S) as a search model. The initial model of PfADF1 was subject to automatic building using ARP/wARP (8) before the structure was completed by further cycles of manual building and refinement using COOT (9) and Phenix (10), respectively. Structure validation was carried out using MolProbity (11). Data collection and refinement statistics for PfADF1 are presented in Table S1. The coordinate and structure factors are available from the Protein Data Bank (PDB ID 3Q2B). Structural alignment and structural-based sequence alignment were generated using the program MUSTANG (12). Secondary structure elements were calculated using stride (13). Structural figures were prepared using PyMol (Delano Scientific LLC, http://www.pymol.org).

Electron Microscopy. Rabbit actin (1 μM) (Cytoskeleton, Inc.) was polymerized by addition of 1/10th volume of 10× F buffer and incubated for 1 h at room temperature. PfADF1 and PfADF1. K72A mutant (30 nM and 250 μM) were added to preformed filaments and incubated at room temperature for 5 min to induce severing. Solutions were adsorbed for 20 s on Formvar-carbon films supported on 200-mesh copper grids. Grids were glow discharged before being negatively stained for 30 s with 1.5%

aqueous uranyl acetate. Samples then were observed with an FEI Tecnai F30 at 300 kV or a Philips CM120 at 120-kV electron microscopes. Data were acquired for all of the actin filaments present in one square of each grid per sample. Filament length was measured using the Segmented Lines tool from ImageJ (http://rsb.info.nih.gov/ij/).

Total Internal Reflection Fluorescence Microscopy. TIRF images of a mixture of 1.33 μM Mg-ATP-actin supplemented with 0.67 μM Oregon Green-labeled Mg-ATP-actin excited by evanescent wave fluorescence were acquired every 10 seconds on an IX-71 microscope (Olympus) fit with through-the-objective TIRF illumination and an iXon EMCCD camera (Andor Technology), as described (14). Filaments were assembled until they reached ~10 μm in length. Then 1.8 chamber-volumes (18 μL) of TIRF buffer [10 mM imidazole (pH 7.0), 50 mM KCl, 5 mM $MgCl_2$, 1 mM EGTA, 0.5 mM DTT, 0.2 mM ATP, 50 μM $CaCl_2$, 15 mM glucose, 20 μg/mL catalase, 100 μg/mL glucose oxidase, 0.5% methylcellulose (500 cP)], PfADF1, SpCOF, HsCOF, or protein mutants were introduced into the chamber by capillary action during continuous imaging. Final protein concentrations are indicated in figure legends.

1. Riglar DT, et al. (2011) Super-resolution dissection of coordinated events during malaria parasite invasion of the human erythrocyte. *Cell Host Microbe* 9:9–20.
2. Richard D, et al. (2010) Interaction between *Plasmodium falciparum* apical membrane antigen 1 and the rhoptry neck protein complex defines a key step in the erythrocyte invasion process of malaria parasites. *J Biol Chem* 285:14815–14822.
3. Baum J, et al. (2006) A conserved molecular motor drives cell invasion and gliding motility across malaria life cycle stages and other apicomplexan parasites. *J Biol Chem* 281:5197–5208.
4. Healer J, Crawford S, Ralph S, McFadden G, Cowman AF (2002) Independent translocation of two micronemal proteins in developing *Plasmodium falciparum* merozoites. *Infect Immun* 70:5751–5758.
5. de Koning-Ward TF, et al. (2009) A newly discovered protein export machine in malaria parasites. *Nature* 459:945–949.
6. Long F, Vagin AA, Young P, Murshudov GN (2008) BALBES: A molecular-replacement pipeline. *Acta Crystallogr D Biol Crystallogr* 64:125–132.
7. Vagin A, Teplyakov A (2010) Molecular replacement with MOLREP. *Acta Crystallogr D Biol Crystallogr* 66:22–25.
8. Morris RJ, Perrakis A, Lamzin VS (2002) ARP/wARP's model-building algorithms. I. The main chain. *Acta Crystallogr D Biol Crystallogr* 58(Pt 6 Pt 2):968–975.
9. Emsley P, Cowtan K (2004) Coot: Model-building tools for molecular graphics. *Acta Crystallogr D Biol Crystallogr* 60(Pt 12 Pt 1):2126–2132.
10. Adams PD, et al. (2002) PHENIX: Building new software for automated crystallographic structure determination. *Acta Crystallogr D Biol Crystallogr* 58:1948–1954.
11. Davis IW, et al. (2007) MolProbity: All-atom contacts and structure validation for proteins and nucleic acids. *Nucleic Acids Res* 35(Web Server issue):W375–383.
12. Konagurthu AS, Whisstock JC, Stuckey PJ, Lesk AM (2006) MUSTANG: A multiple structural alignment algorithm. *Proteins* 64:559–574.
13. Frishman D, Argos P (1995) Knowledge-based protein secondary structure assignment. *Proteins* 23:566–579.
14. Neidt EM, Skau CT, Kovar DR (2008) The cytokinesis formins from the nematode worm and fission yeast differentially mediate actin filament assembly. *J Biol Chem* 283:23872–23883.

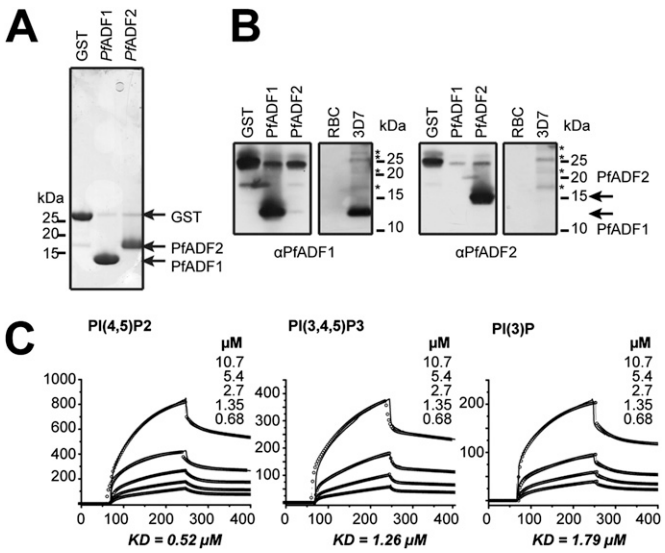

Fig. S1. Specificity of antisera raised against recombinant PfADF1 and PfADF2. (*A*) SDS/PAGE analysis of the purified recombinant PfADF1 and PfADF2. (*B*) Immunoblot showing the specificity of the αPfADF1 and αPfADF2 antibodies. RBC, red blood cell lysate, 3D7, wild-type 3D7 strain of *P. falciparum* lysate. (*C*) Biacore analysis of the interaction of recombinant PfADF1 with immobilized phosphatidylinositol 4,5-bisphosphate [PI(4,5)P2], phosphatidylinositol (3,4,5)-trisphosphate [PI(3,4,5)P3], and phosphatidylinositol 3-phosphate [PI(3)P]. Various concentrations of cofilin (10.7 μM, 5.4 μM, 2.7 μM, 1.35 μM, and 0.68 μM) were injected over biotin derivatives of PI(4,5)P2, PI(3,4,5)P3, and PI(3)P immobilized onto NeutrAvidin. The amounts of phosphoinositide immobilized were ~160 relative units (RU), 280 RU, and 240 RU for PI(4,5)P2, PI(3,4,5)P3, and PI(3)P, respectively. The sensorgrams shown have had the corresponding signal obtained when the sample was passed over a NeutrAvidin channel subtracted.

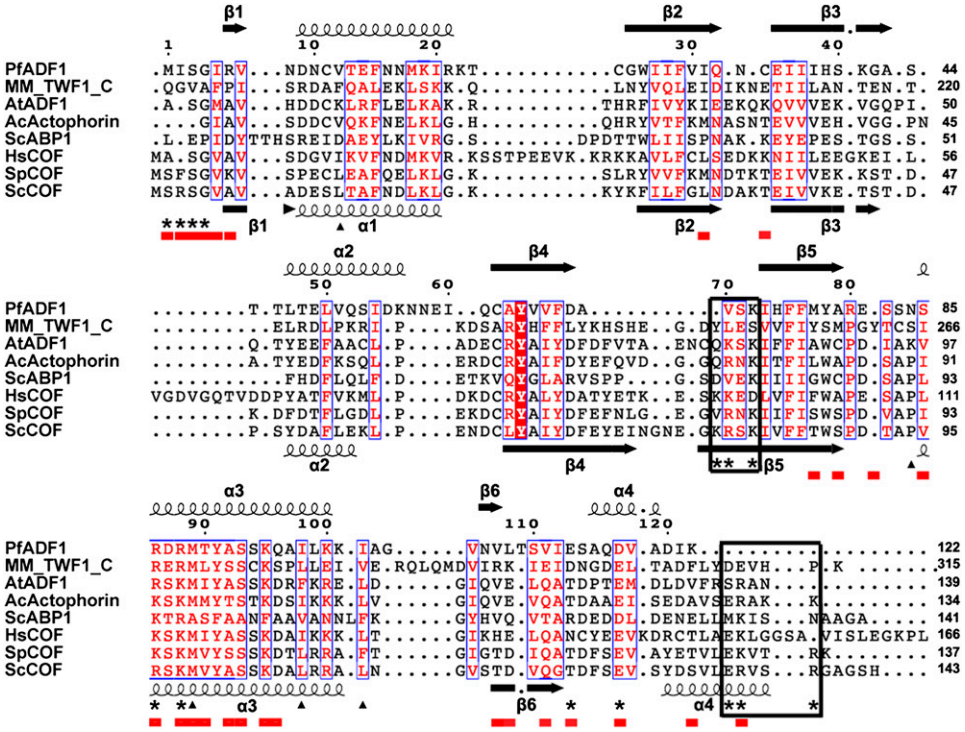

Fig. S2. Structure-based sequence alignment of AC family members. MM_TWF1_C, mouse twinfilin C-terminal domain; AtADF1, *Arabidopsis thaliana* actin-depolymerizing factor; AcActophorin, *Acanthamoeba castellani* actophorin; ABP1, *Saccharomyces cerevisiae* actin-binding protein 1; HsCOF, *Homo sapiens* cofilin; SpCOF, *Schizosaccharomyces pombe* cofilin; and ScCOF, *S. cerevisiae* cofilin. Residue numbers follow PfADF1. Secondary structural elements present in PfADF1 and ScCOF are shown above and below alignment respectively. Actin-binding sites identified by mutagenesis or synchrotron protein-footprinting are indicated by asterisks and arrowheads, respectively (1–3). Actin-binding sites identified in mouse TWF1_C-actin complex are underlined in red. Residues implicated exclusively in F-actin binding are boxed in black (2, 3). Strictly conserved residues are highlighted by red shading. Homologous residues are highlighted in red text.

1. Guan JQ, Vorobiev S, Almo SC, Chance MR (2002) Mapping the G-actin binding surface of cofilin using synchrotron protein footprinting. *Biochemistry* 41:5765–5775.
2. Lappalainen P, Fedorov EV, Fedorov AA, Almo SC, Drubin DG (1997) Essential functions and actin-binding surfaces of yeast cofilin revealed by systematic mutagenesis. *EMBO J* 16: 5520–5530.
3. Pope BJ, Gonsior SM, Yeoh S, McGough A, Weeds AG (2000) Uncoupling actin filament fragmentation by cofilin from increased subunit turnover. *J Mol Biol* 298:649–661.

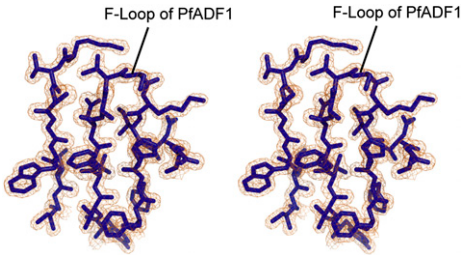

Fig. S3. The short F-loop of PfADF1. Stereo view of a $2|F_o|-|F_c|$ electron density map depicting the short F-loop of PfADF1. The map is contoured at 1.2 σ. Water molecules have been removed for clarity.

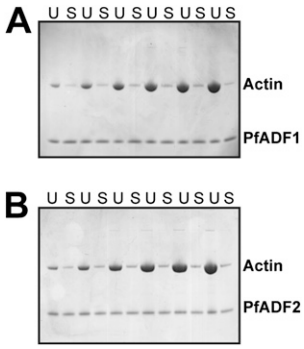

Fig. S4. Pelleting assay to determine the dissociation equilibrium constant of PfADF1 and rabbit actin filaments. Ultracentrifugation of 5 μM PfADF1 (*A*) or PfADF2 (*B*) with varying concentrations of preformed filaments with an equal amount of uncentrifuged and postcentrifuged supernatant analyzed by SDS/PAGE and densitometry. S, supernatant; U, uncentrifuged sample.

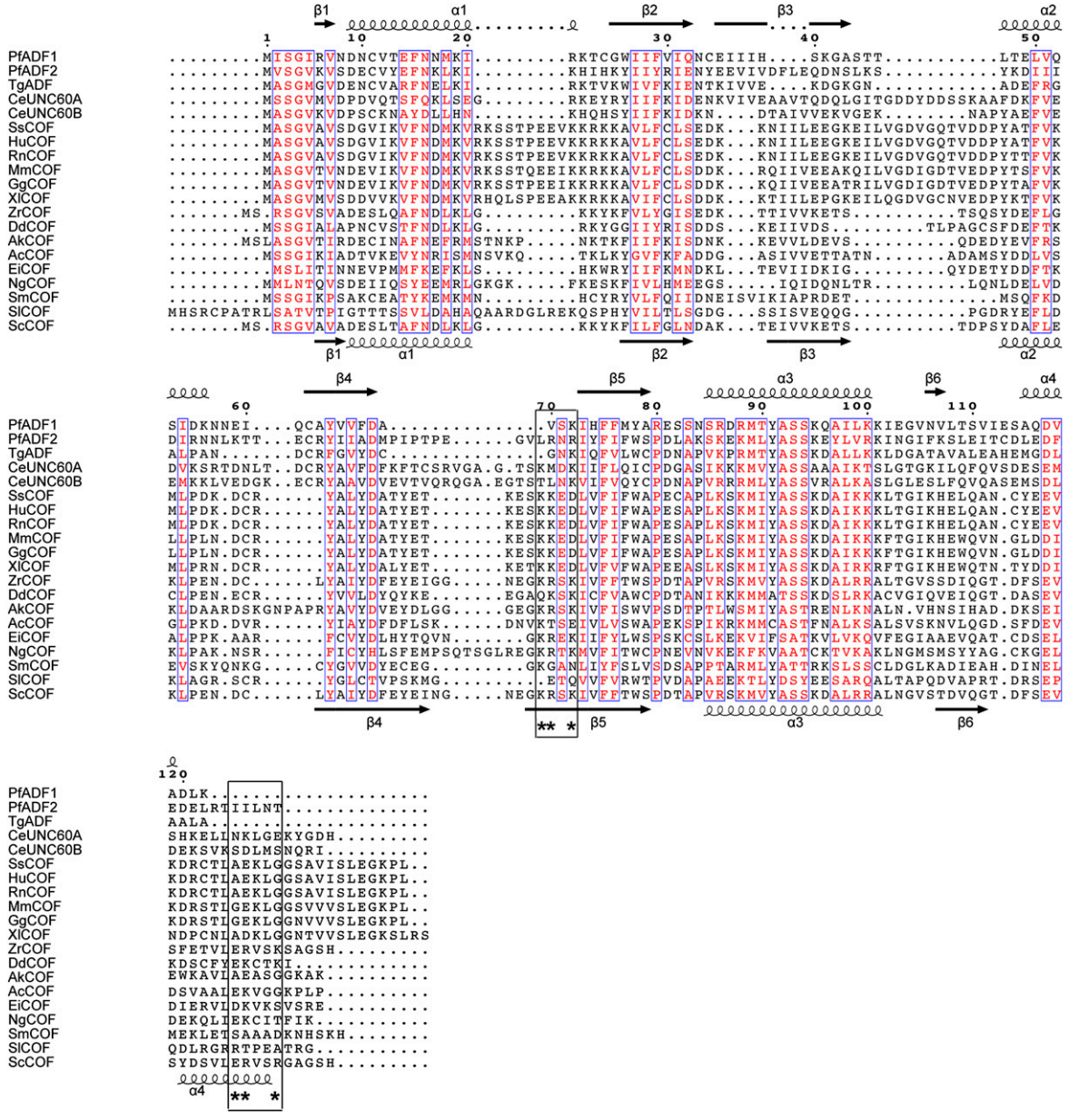

Fig. S5. ClustalX-generated sequence alignment of AC family members. Sequences shown are PfADF1 and PfADF2 from *P. falciparum*; TgADF from *Toxoplasma gondii*; CeUNC60A and B from *Caenorhabditis elegans*; SsCOF from *Sus scrofa*; HuCOF from *Homo sapiens*; RnCOF from *Rattus norvegicus*; MmCOF from *Mus musculus*; GgCOF from *Gallus gallus*; XlCOF from *Xenopus laevis*; ZrCOF from *Zygosaccharomyces rouxii*; DdCOF from *Dictyostelium discoideum*; AkCOF from *Aplysia kurodai*; AcCOF from *Aspergillus clavatus*; EiCOF from *Entamoeba invadens*; NgCOF from *Naegleria gruberi*; SmCOF from *Schistosoma mansoni*; SlCOF from *Streptomyces lavendulae*; and ScCOF from *S. cerevisiae*. Secondary structure elements present in PfADF1 and ScCOF are shown above and below the alignment, respectively, with residue numbers at the top of the alignment following PfADF1. Residues required exclusively for F-actin binding are boxed in black and marked by asterisks. Homologous residues are highlighted in red text.

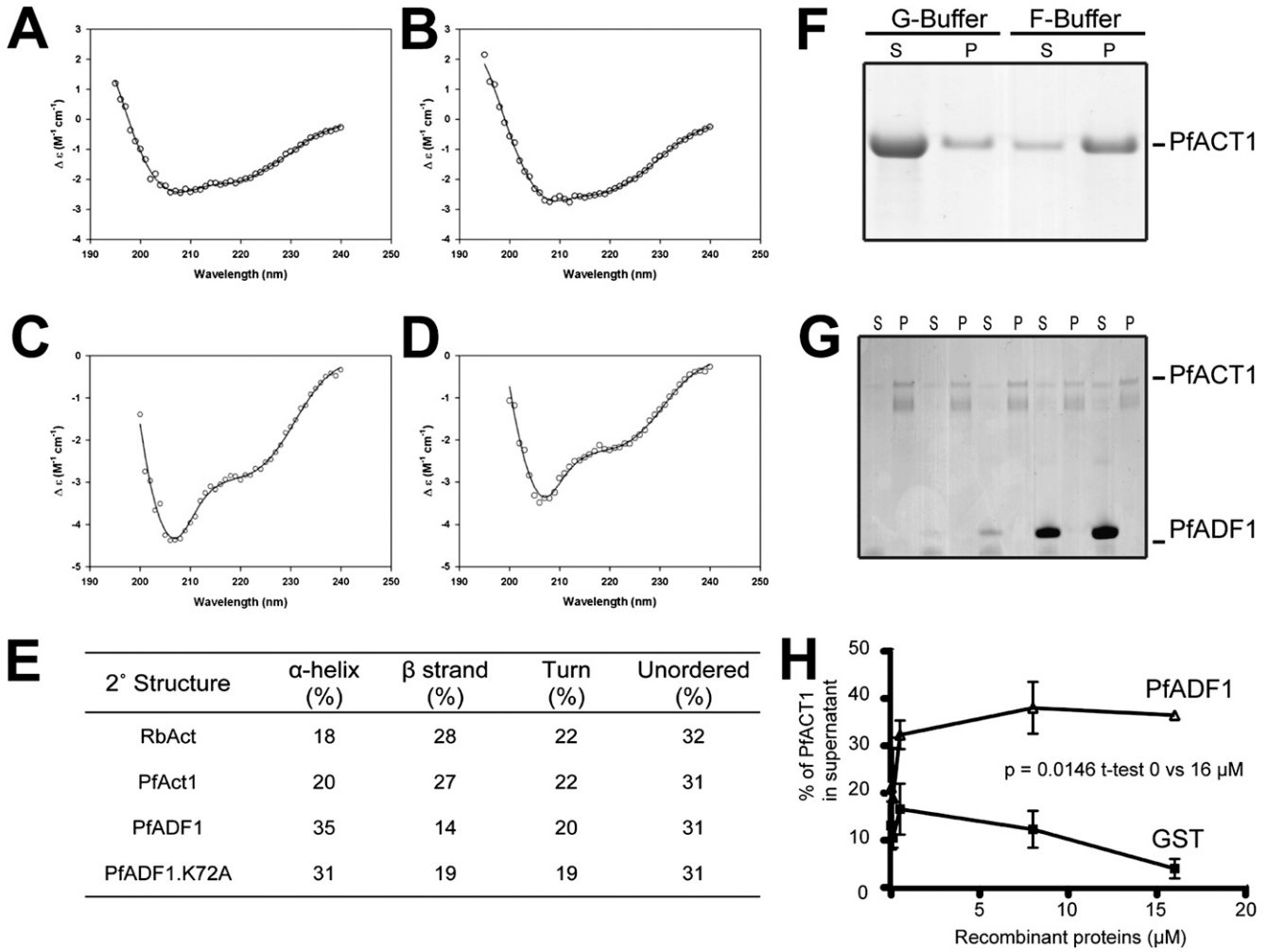

E

2° Structure	α-helix (%)	β strand (%)	Turn (%)	Unordered (%)
RbAct	18	28	22	32
PfAct1	20	27	22	31
PfADF1	35	14	20	31
PfADF1.K72A	31	19	19	31

Fig. S6. Biophysical and biochemical characterization of recombinant PfAct1 and PfADF1.K72A mutant. (*A–D*) Circular dichroism spectra and the change in extinction coefficient ($\Delta\varepsilon$) is plotted as a function of wavelength for (*A*) RbAct, (*B*) PfAct1, (*C*) PfADF1, and (*D*) PfADF1.K72A. The data (open circles) shown are the average result from three scans taken at 20 °C, and the solid lines represent the nonlinear least squares regression analysis best fits using the CONTINLL algorithm from the CDPro software package using the SP43 protein database (1). The fits resulted in rmsd values of 0.119, 0.084, 0.110, and 0.101 for rabbit actin (RbAct), PfAct1, PfADF1, and PfADF1.K72A, respectively. (*E*) Secondary structure proportions of RbAct, PfAct1, PfADF1, and PfADF1.K72A calculated by nonlinear regression analyses of CD spectral data shown in *A–D* using the SP43 database and CONTINLL algorithm. (*F*) Ultracentrifugation of PfAct1 prepared under nonpolymerizing (G-Buffer) and polymerization condition (F-Buffer) with equal amounts of supernatant and pellet fractions analyzed by SDS/PAGE. (*G*) Ultracentrifugation of PfADF1 with preformed PfAct1 filaments. GST control is included. P, pellet; S, supernatant. (*H*) Quantification of proportion of actin in respective fractions from *G*. Data shown represent mean ± SEM for $n = 3$.

1. Sreerama N, Venyaminov SY, Woody RW (2000) Estimation of protein secondary structure from circular dichroism spectra: inclusion of denatured proteins with native proteins in the analysis. *Anal Biochem* 287(2):243–251.

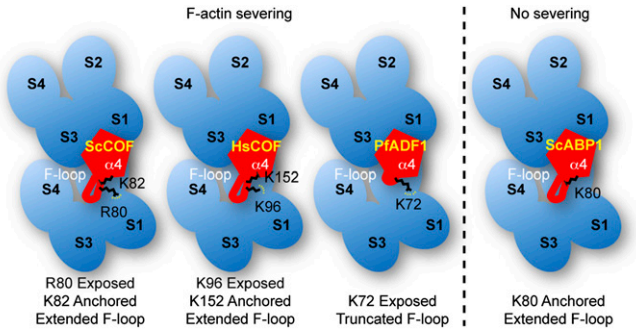

Fig. S7. Model of minimal requirements for actin filament severing across representative members of the AC family. The ability of an AC protein to mediate filament severing depends on the availability of an exposed basic residue in the F-loop of the protein. Importantly, the orientation of the exposed basic residue must positions toward the α4 helix for severing to occur. Note that ScCOF, HsCOF and PfADF1 all have minimally one exposed basic residue, which confers the ability to sever filaments irrespective of the size of the F-loop. In contrast, the only basic residue (Lys^{80}) in the F-loop of *S. cerevisiae* actin-binding protein 1 (ScABP1) is anchored by the α4 helix and therefore is unavailable for severing. Actin monomers are represented in blue with subdomains labeled. AC proteins are represented in red with the F-loop, α4 helix, and basic residues labeled.

Table S1. Data collection and structure refinement statistics

Wavelength (Å)	0.95369
Space group	$P4_32_12$
Unit-cell parameters (Å, °)	*a*, *b* = 38.97Å, *c* = 142.40Å, α, β, γ = 90°
Resolution range (Å)	50.0–1.6 (1.66–1.6)
Multiplicity	13.5 (13.6)
Unique reflections	15439 (1494)
I/σ(I)	36 (3.2)
Completeness (%)	99.9 (99.9)
Rmerge*	0.067 (0.999)
Resolution (Å)	27.6–1.6
R_{work}/R_{free}†	19.3/21.8
No. atoms	
Protein	981
Water	78
Solvent	104
B-factors	
Protein	29.1
Water	38.6
Rms deviations	
Bond length (Å)	0.009
Bond angles (°)	1.203
Ramachandran plot (%)	
Favored region	98.6
Allowed region	1.4
Disallowed region	0
MOLPROBITY score	1.6

Values in parentheses are for the highest-resolution shell.

*Rmerge = $\sum_{hkl} \sum_i |I_i(hkl) - (I(hkl))| / \sum_{hkl} \sum_i I_i(hkl)$, where $I_i(hkl)$ and $(I(hkl))$ represent the diffraction-intensity values of the individual measurements and the corresponding mean values.

†R = $\sum$ |Fobs – Fcalc|/$\sum$Fobs, where Rfree is calculated with the 5% of data omitted from the refinement and Rwork with the remaining 95% of the data included in the refinement.

Table S2. Secondary structure proportions of RbAct, PfAct1, PfADF1, PfADF1.K72A calculated by nonlinear regression analyses of CD spectral data (Fig. S7) using the SP43 database and CONTINLL algorithm

Secondary structure	α-helix (%)	β strand (%)	Turn (%)	Unordered (%)
RbAct	18	28	22	32
PfAct1	20	27	22	31
PfADF1	35	14	20	31
PfADF1.K72A	31	19	19	31

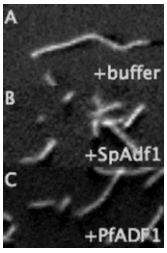

Movie S1. Time-lapse TIRF microscopy of filament growth and severing in the presence of PfADF1, SpCOF, and buffer only (from Fig. 4).

Movie S1